Journal of Marine Systems 76 (2009) 383–396

Contents lists available at ScienceDirect

Journal of Marine Systems

journal homepage: www.elsevier.com/locate/jmarsys

Turbulent mixing and internal tides in Gaoping (Kaoping) Submarine Canyon, Taiwan

I-Huan Lee [a,1], Ren-Chieh Lien [b], James T. Liu [a,*], Wen-ssn Chuang [c]

[a] Institute of Marine Geology and Chemistry, National Sun Yat-sen University, Kaohsiung, Taiwan 804-24, ROC
[b] Applied Physics Laboratory, University of Washington, Seattle, WA 98105, USA
[c] Institute of Oceanography, National Taiwan University, Taipei, Taiwan 106, ROC

ARTICLE INFO

Article history:
Received 9 February 2007
Received in revised form 17 August 2007
Accepted 30 August 2007
Available online 23 August 2008

Keywords:
Turbulent mixing
Internal tides
Sediment Flux
Submarine Canyon

ABSTRACT

Turbulent overturning on scales greater than 10 m is observed near the bottom and in mid-depth layers within the Gaoping (formerly spelled Kaoping) Submarine Canyon (KPSC) in southern Taiwan. Bursts of strong turbulence coexist with bursts of strong sediment concentrations in mid-depth layers. The turbulence kinetic energy dissipation rate in some turbulence bursts exceeds 10^{-4} W kg^{-1}, and the eddy diffusivity exceeds 10^{-1} m^2 s^{-1}. Within the canyon, the depth averaged turbulence kinetic energy dissipation rate is ~7×10^{-6} W kg^{-1}, and the depth averaged eddy diffusivity is ~10^{-2} m^2 s^{-1}. These are more than two orders of magnitude greater than typical values in the open ocean, and are much larger than those found in the Monterey Canyon where the strong turbulent mixing has also been. The interaction of tidal currents with the complex topography in Gaoping Submarine Canyon is presumably responsible for the observed turbulent overturning via shear instability and the breaking of internal tides and internal waves at critical frequencies. Strong 1st-mode internal tides exist in KPSC. The depth averaged internal tidal energy near the canyon mouth is ~0.17 m^2 s^{-2}. The depth integrated internal tidal energy flux at the mouth of the canyon is ~14 kW m^{-1}, propagating along the axis of the canyon toward the canyon head. The internal tidal energy flux in the canyon is 3–7 times greater than that found in Monterey Canyon, presumably due to the more than 10 times larger barotropic tide in the canyon. Simple energy budget calculations conclude that internal tides alone may provide energy sufficient to explain the turbulent mixing estimated within the canyon. Further experiments are needed in order to quantify the seasonal and geographical distributions of internal tides in Gaoping Submarine Canyon and their effects on the sediment flux in the canyon.

1. Introduction

Submarine canyons are natural traps of suspended fine-grained sediments. Turbulent entrainment of sediments from the seabed within the water column facilitates the transport of suspended sediments by currents inside submarine canyons. Therefore, submarine canyons are potential conduits for the sediment flux between the shelf and deep ocean. Internal tides and associated turbulent processes have been shown not only to create and maintain nepheloid layers, but also to transport suspended sediments (Friedrichs and Wright, 1995). Liu et al. (2002) find strong inhomogeneity of suspended sediment concentration (SSC) in a submarine canyon. They hypothesize that observed pockets of high SSC are caused by breaking internal tides trapped in the submarine canyon.

Tidal currents dominate the flow field in many submarine canyons (Shepard et al., 1974, 1979; García Lafuente et al.,

* Corresponding author.
E-mail addresses: ihlee@mail.nsysu.edu.tw (I.-H. Lee), lien@apl.washington.edu (R.-C. Lien), james@mail.nsysu.edu.tw (J.T. Liu), chuang@ntu.edu.tw (W. Chuang).
[1] Present address: National Museum of Marine Biology and Aquarium, Pingtung, Taiwan 94450, ROC.

0924-7963/$ – see front matter © 2008 Elsevier B.V. All rights reserved.
doi:10.1016/j.jmarsys.2007.08.005

1999; Xu et al., 2002). The vertical stratification and the complex topography in submarine canyons (Monaco et al., 1990; Liu et al., 2002) favor the generation and focusing of internal tides (Hotchkiss and Wunsch, 1982; Petruncio et al., 1998; Cresswell, 2000; Jachec et al., submitted for publication). The internal tidal energy propagates primarily along the canyon axis due to the topographic steering. A broad spectrum of turbulent processes exists in submarine canyons such as the bottom boundary-layer turbulence and turbulence generated by breaking of internal waves and internal tides (Carter and Gregg, 2002). At critical slopes, the enhancement of internal waves of critical frequencies, whose characteristic slopes match the slope of the ocean bottom, could cause resuspension and deposition of sediment. Ribbe and Holloway (2001) report a strong on-shelf sediment transport associated with internal tides.

In the deep open ocean, free linear internal waves are well modeled by the GM spectrum (Garrett and Munk 1972, 1975). Near sources and sinks of internal waves, observed spectra deviate from the GM spectrum. Most deviations from the GM spectrum are found near topography such as shelf breaks, continental slopes, and submarine canyons (Wunsch 1976; Wunsch and Webb 1979; Hotchkiss and Wunsch 1982; Lien et al., 2005).

This study in Gaoping (formerly spelled Kaoping) Submarine Canyon quantifies the turbulent mixing, associated energy dissipation rate, internal tidal energy and energy flux, and examines the possible link between turbulent mixing and small-scale suspended sediment anomalies in the canyon. In Section 2, we describe the experiment and the measurements, and present brief summary of previous observations of sediment concentration. In Section 3, we compare the internal wave continuum in the canyon with the prediction by the GM spectrum, and compute internal tidal energy and energy flux. In Section 4, we compute the turbulent overturning scales, turbulence kinetic energy dissipation rate, and eddy diffusivity within the canyon. Possible explanations for intermediate and near-bottom nepheloid layers are discussed. Results of this analysis are summarized in Section 5.

2. Experiment, measurements, and previous results

2.1. Experiment site

The study site, Gaoping Submarine Canyon, is located in southern Taiwan on a wave-dominated microtidal (tidal range smaller than 2 m) coast (Fig. 1a). The head of the canyon is located approximately 1 km off the mouth of Gaoping River whose physical setting has been described in detail by Liu et al. (2002).

2.2. Measurements

Comprehensive field experiments were carried out between June 1999 and July 2000 onboard the *R/V* Ocean Researcher III to study the sediment flux in the canyon. These two experiments consisted of (1) 8 one-day cruises of hydrographic vertical profiles along the axis (10 stations labeled as A–J in Fig. 1) of the canyon within 10 km from the canyon head, (2) twelve hourly hydrographic vertical profiles at a fixed site at the center of the canyon axis (the vertical white line), and (3) one-month long current meter measurements at 200- and 270-m depths on a mooring (the vertical white line) between June 20 and July 20, 2000. Details of the experiment, instruments, measurements, and data processing are described in Liu et al. (2002).

Dates of the 8 cruises are labeled in Fig. 2. Ten stations, from station A at the head of the canyon to the offshore station J (Fig. 1b), are occupied during each survey. At each station, profiles of conductivity, temperature, and light transmission were measured using a Sea Bird SBE 9/11 CTD system at ~0.2 m vertical intervals from surface to about 20 m above the seafloor.

A set of 28 h of hourly shipboard ADCP and CTD vertical profiles were taken on Feb. 26–27, 2004 (the red line in Fig. 1b and the cross in Fig. 1a). Internal tidal energy and energy flux were estimated using these data, providing basic properties of internal tides in the canyon.

2.3. Previous results of suspended sediment concentration (SSC) observations

Gaoping Submarine Canyon is stably stratified by temperature (Liu et al., 2002). The deeper part of the canyon is filled with colder and more saline offshore water that is little affected by the change of seasons. The water column is stable in the summer river flood season and less stable during the dry winter season. During the transition in fall, the upper part of the canyon remains highly stable but the deeper part becomes less stable.

Measurements of light transmission along the canyon axis are shown in Fig. 2. It takes 4–5 h to complete one hydrographic profiling transect. Observed hydrographic fluctuations along each transect are modulated by tides at varying phases. Therefore, Fig. 2 represents tidally aliased quasi-snapshots of light transmission along the canyon axis.

Hydrographic surveys were conducted during flood seasons (cruises 1, 2, 7, and 8), dry seasons (cruises 5 and 6), and transitions (cruises 3 and 4). Liu et al. (2002) infer suspended sediment concentrations from light transmission measurements. Observed suspended sediment concentration distributions exhibit common characteristics: (1) High suspended sediment concentration values are generally in the lower part of the water column. Except for the two flood season surveys, higher suspended sediment concentration values also tend to occur toward the seaward end of the canyon. (2) During the flood season, higher concentrations of suspended sediments carried by the river effluent are evident near the surface toward the head of the canyon. (3) There are localized patches of high suspended sediment concentrations. These patches sometimes coexist with localized density inversions. Since these patches exist in the vicinity where internal M_2 tides may be generated or reflected, Liu et al. (2002) propose that high suspended sediment concentration patches are associated with the trapping internal tidal energy without any quantifying evidence.

In laboratory experiments, McPhee-Shaw and Kunze (2002) demonstrate that reflection of internal waves from a sloping boundary not only could cause instabilities and create density perturbations, it also could cause intrusions of dyed fluid from the boundary following isopycnal surfaces.

3. Internal waves and internal tides

3.1. Internal waves in Gaoping Submarine Canyon versus GM prediction

Frequency spectra of horizontal kinetic energy (HKE) are computed using two current meters. Peaks are present at the semidiurnal (ω=0.0805 cph) and diurnal (ω=0.042 cph) frequencies (Fig. 3). There is a secondary peak at twice the semidiurnal tidal frequency (ω=0.16 cph), suggesting nonlinearity of semidiurnal tides. The semidiurnal tide is stronger than the diurnal tide. In the internal wave continuum, ω>0.2 cph, spectra exhibit the canonical "−2" slope. The observed kinetic energy is about 3 times the prediction by the GM internal wave model. Hotchkiss and Wunsch (1982) found a similar increase of internal wave energy toward the head of Hudson Canyon.

Frequency spectra of the clockwise and counterclockwise rotating vertical shears are computed, having similar magnitudes. For linear internal waves in the northern hemisphere, the clockwise rotating vertical shear is greater than the counterclockwise rotating shear. Our observed equipartition

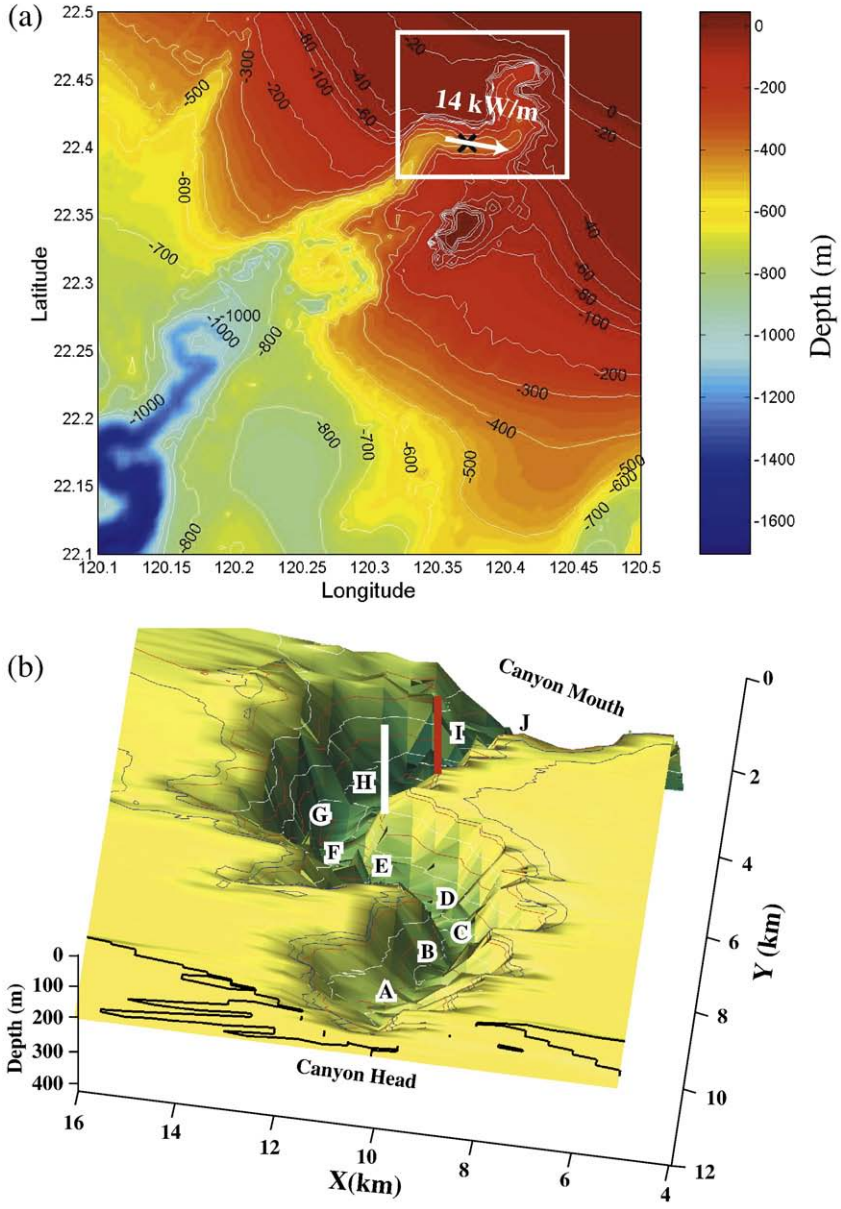

Fig. 1. (a) Bathymetric map of Gaoping Submarine Canyon in southern Taiwan and (b) the 3-d perspective of Gaoping Submarine Canyon looking from the head to the mouth, roughly corresponding to the white box in (a). The nominal positions of 10 along-canyon stations are labeled A–J. The vertical white bar marks the location of the 12-h profiling of CTD, near the mooring of two current meters. The black cross in (a) and the vertical red line in (b) mark the location of 28 h of ADCP and CTD profiles taken during Feb. 26–27 of 2004. The white arrow in (a) shows the depth-integrated internal tidal energy flux computed in Section 3.

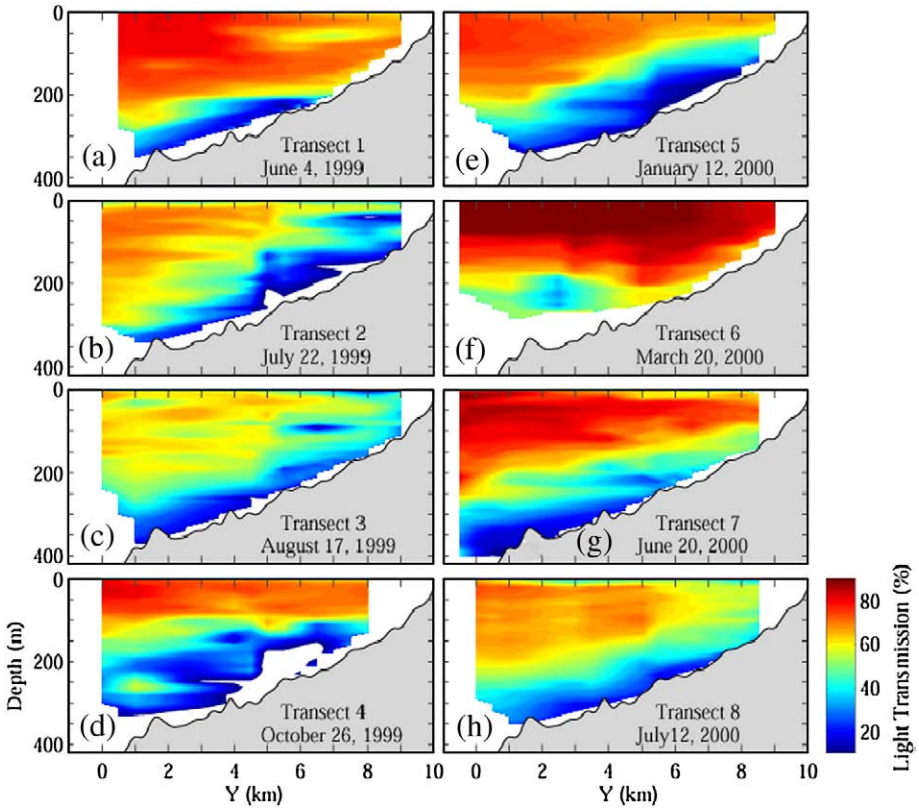

Fig. 2. Light transmission observations during 8 transects along the canyon axis. Dates of cruises are labeled.

of the two rotary shear components is inconsistent with free linear internal waves. This departure suggests the importance of the nonlinearity, external forcing, and boundary effects in Gaoping Submarine Canyon. Primary shear spectral peaks are at the diurnal, semidiurnal, and 6-h tidal frequencies. There is no significant spectral peak at the inertial frequency (ω=0.032 cph). The narrow width of the canyon likely suppresses inertial waves (Hotchkiss and Wunsch, 1982).

In the canyon, the energy of background internal waves is three times greater than that predicted by the GM model. Strong internal tides could be generated in the canyon (discussed in the next section), and background internal waves enhanced via the wave–wave interaction and critical slope processes.

3.2. Internal tidal energy and energy flux in Gaoping Submarine Canyon

Continuous vertical profiles of CTD and shipboard 75-kHz ADCP measurements were taken hourly for 28 h in 2004 near the canyon mouth at ~350 m depth. The vertical normal mode

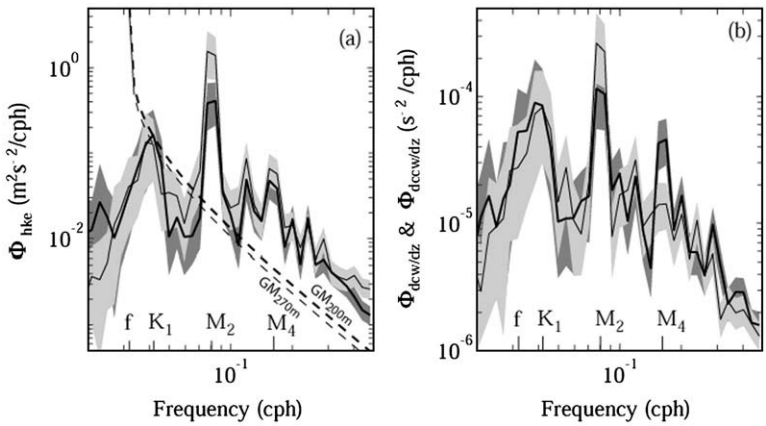

Fig. 3. (a) Frequency spectra of horizontal kinetic energy (HKE) at 200-m depth (thick solid) and at 270-m depth (thin solid), and (b) observed vertical shear of clockwise (thick solid) and counterclockwise velocity (thin solid) between 200- and 270-m depths. Shadings indicate 95% confidence intervals. In panel (a), thick and thin dashed curves represent horizontal kinetic energy spectra predicted by the GM model at 200- and 270-m depths, respectively. Frequencies of inertial (f), diurnal (K_1), and semidiurnal (M_2) frequencies are labeled.

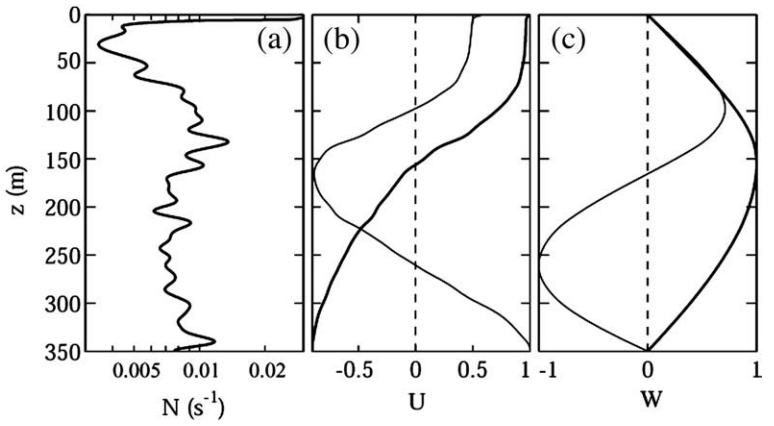

Fig. 4. Vertical profiles of (a) buoyancy frequency, (b) vertical structures of the first two vertical modes of horizontal velocity, and (c) vertical structures of the first two vertical modes of vertical velocity. Thick curves in (b) and (c) represent the first mode, and thin curves represent the second mode.

structures of internal tides are computed using the average of the sorted density profiles (Fig. 4). The buoyancy frequency is mostly between 0.008 and 0.01 s^{-1}. The first mode of horizontal velocity had a nodal point at ~150 m depth. The phase propagation speed C_p of internal tides of the lowest two modes is 1, and 0.5 m s^{-1}, respectively. The energy speed,

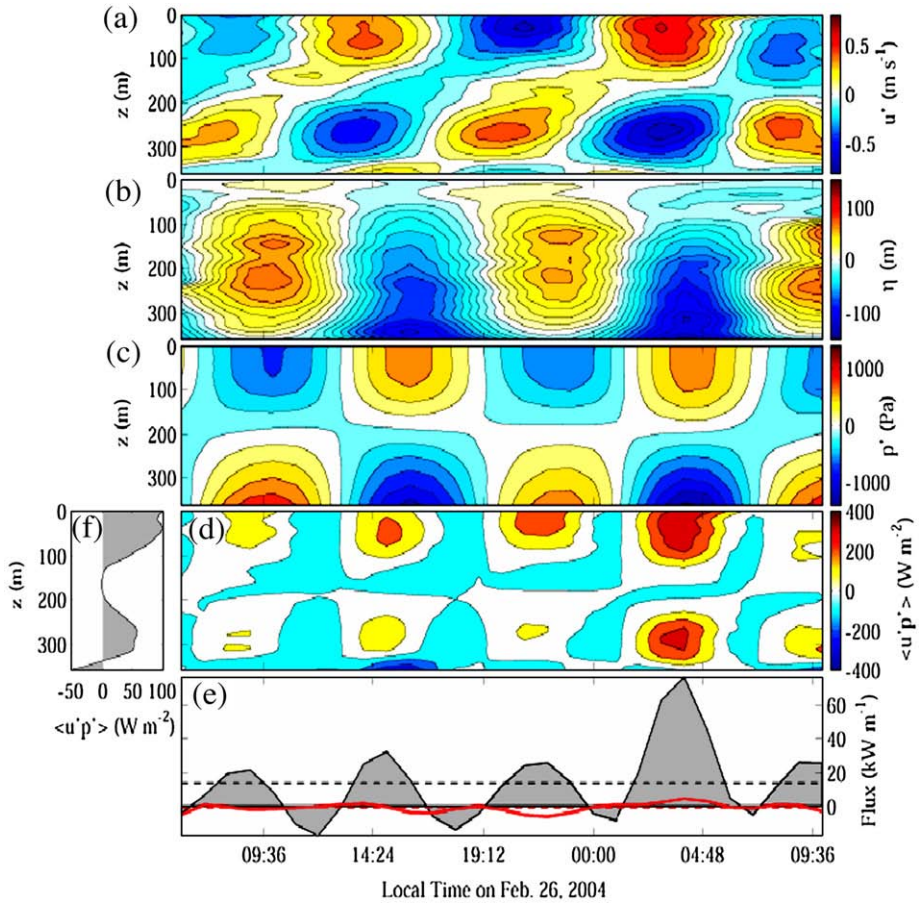

Fig. 5. Vertical and temporal variations of (a) the zonal velocity perturbations, (b) the isopycnal vertical displacements, (c) the pressure perturbation with the hydrostatic component and vertical mean removed, and (d) the zonal energy flux. The vertically integrated zonal energy flux (black curve with shading) and meridional energy flux (red curve) are shown in (e) where the black dashed horizontal line represents the temporal average of vertically integrated zonal energy flux, and the red dashed horizontal line represents the temporal average of vertically integrated meridional energy flux, close to zero. The vertical profile of the temporal average of the zonal energy flux is shown in (f).

$C_g = C_p(\omega^2 - f^2)\omega^{-2} \approx 0.85C_p$, is comparable to the phase speed for semidiurnal internal tides.

We decompose observed velocity vertical profiles into theoretical vertical modes. More than 80% of velocity variance is projected onto the barotropic mode (37%) and the first baroclinic mode (45%). The velocity of the baroclinic tide is ~0.5 m s^{-1} (Fig. 5a). The vertical and temporal average of the baroclinic HKE, mainly internal tides, is 0.04 m^2 s^{-2}.

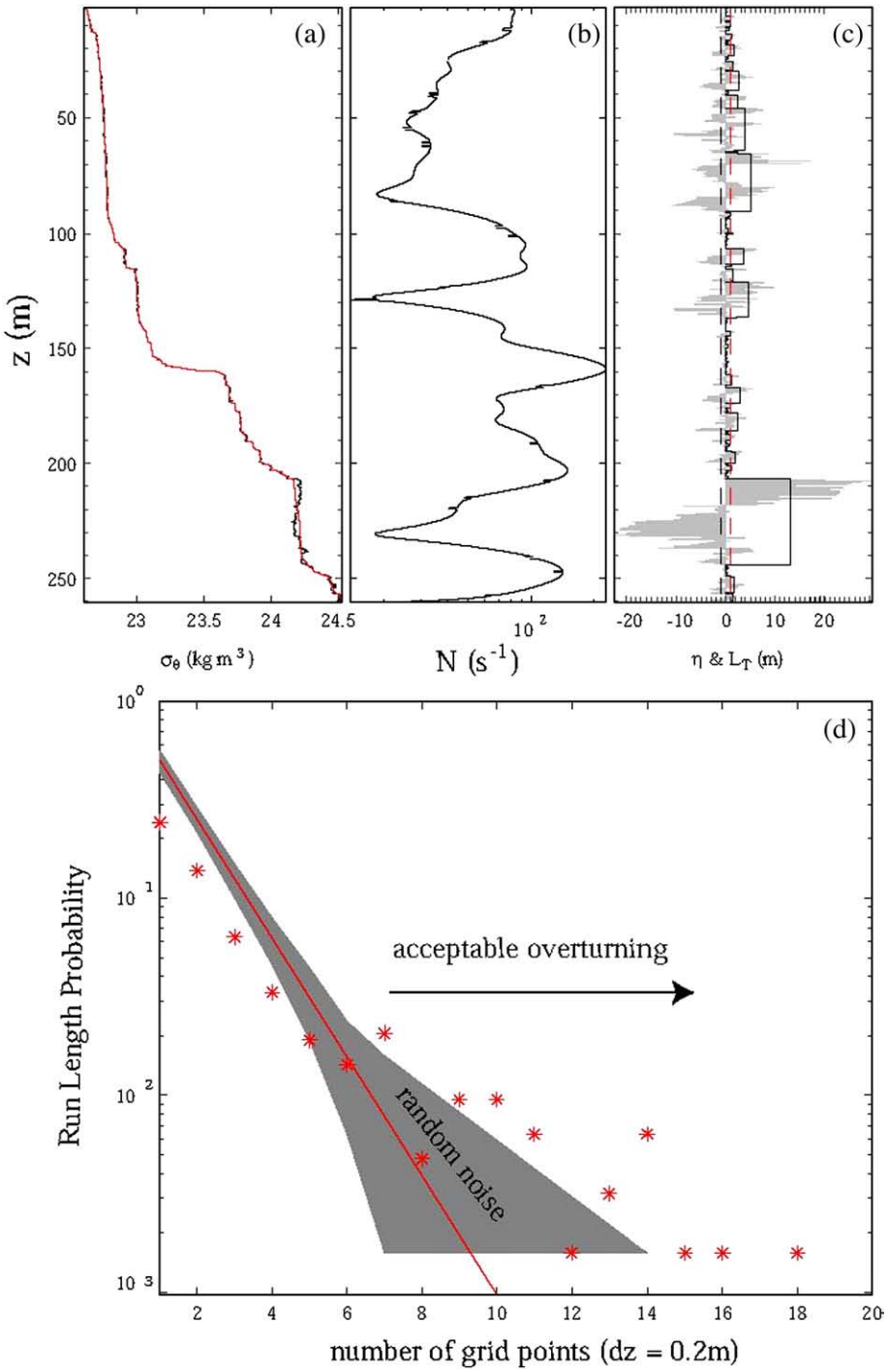

Fig. 6. Illustration of estimates of overturning scales and the run-length test: vertical profiles of (a) observed density (black) and sorted density (red), (b) buoyancy frequency, and (c) Thorpe displacement (shading), and overturning patches (black bar). Magnitudes of bars correspond to the rms Thorpe scale. Panel (d) shows the run-length test. The red line shows the 2^{-n} pdf for random uncorrelated noise, where n is the run-length. The gray shading indicates the 95% confidence computed from the Monte Carlo simulation. Red asterisks represent the pdf of the run-length computed from the observed density profile.

A background potential density profile $\rho_{bg}(z)$ is constructed as follows. We combine the 28-h of vertical profiles of potential density, each with 1-m vertical resolution. We sort the combined potential density profile and assign each density grid with 1/28-m vertical scale so that the sorted combined potential density profile, $\rho_{bg}(z)$, fits into the local water depth. The available potential energy (APE) of the observed baroclinic tide is estimated following Henyey (1983). For every hourly vertical profile the APE is defined as $\mathrm{APE}(z) = \frac{1}{2}N^2(z_0)\eta^2(z)$. The vertical displacement varies mostly between −100 and 70 m, showing a clear tidal fluctuation (Fig. 5b). The vertical and temporal average of APE is 0.13 $m^2\ s^{-2}$. The estimate of the total baroclinic tidal energy, including both diurnal and semidiurnal tides, is 0.17 $m^2\ s^{-2}$. For linear internal waves, APE and HKE have a similar magnitude at frequencies far from N and f. Our findings of APE ~ 3HKE suggest either that observed internal tides are nonlinear or that the vertical displacement of barotropic tides on the sloping bottom is responsible for the excess APE over HKE (Kunze et al., 2002).

The energy flux of internal tides F is computed using simultaneous measurements of density and velocity following Kunze et al. (2002), i.e., $F = EC_g = \langle u'p' \rangle / \rho_0$, where E is the total energy, u' and p' are perturbation velocity and pressure associated with internal waves. The $\langle\ \rangle$ denotes the average over the wave phase. The perturbation pressure is computed using the estimate of vertical displacement. The procedure is described in Kunze et al. (2002). The perturbation pressure

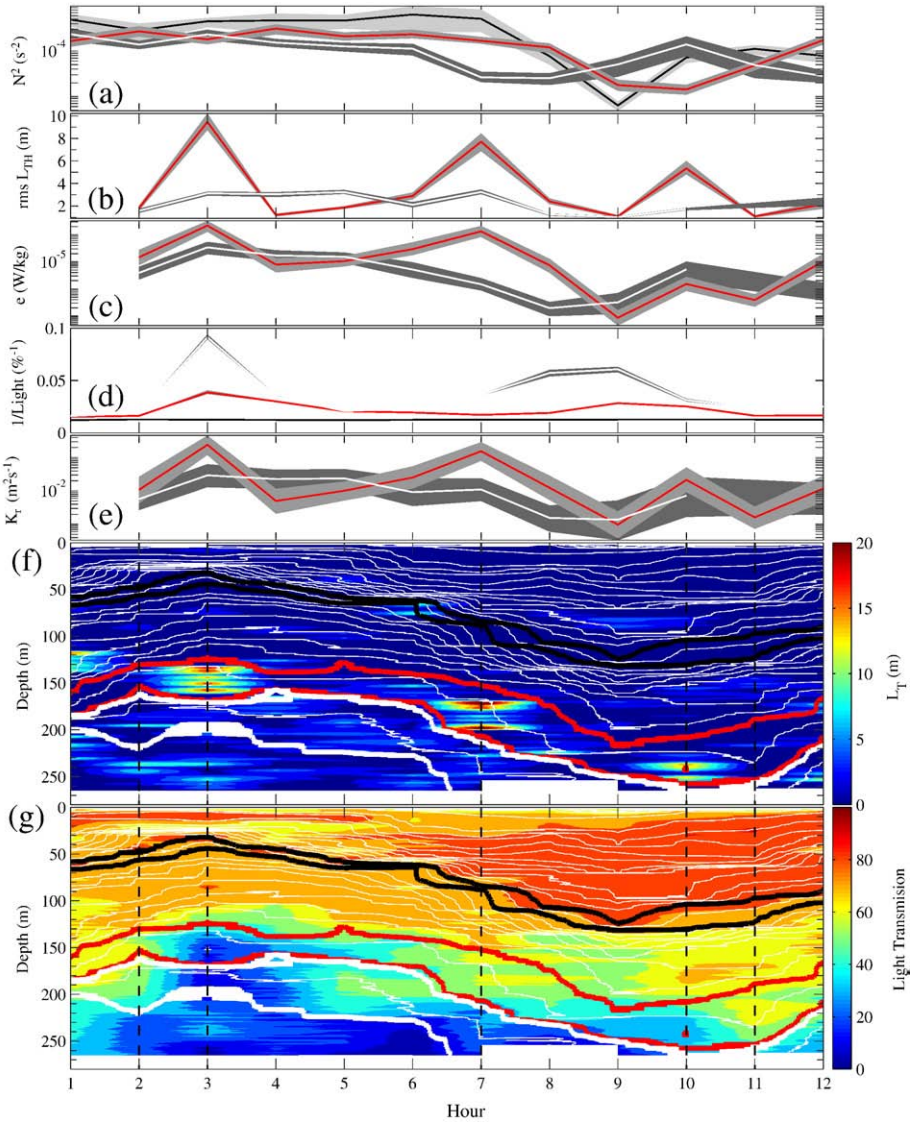

Fig. 7. Time series of (a) N^2, (b) rms Thorpe scale, (c) ε, (d) inverse light transmission, and (e) K_ρ in three density layers: σ_θ=23.2–23.6 (black), σ_θ=25.2–25.6 (red), and σ_θ=26.2–26.6 (white). Shadings are 95% confidence intervals computed using the bootstrap method. Panels (f) and (g) show the contours of rms Thorpe scale and light transmission, respectively. Thin white contour lines are constant σ_θ. Black, red, and white curves mark density layers where time series of variables are averaged and plotted in the top 5 panels. In the lightest density layer (black), since the rms Thorpe scale is smaller than the criterion of the run-length test, estimates of the rms Thorpe scale, ε, and K_ρ are excluded from the following analysis and are not shown in (b), (c), (d) and (e). Vertical black dashed lines denote the times of vertical profiles shown in Fig. 8.

varies mostly between ±600 Pa and shows a clear tidal periodicity (Fig. 5c). The perturbation pressure also shows a dominant first mode structure, similar to that of velocity. The zonal component of the energy flux is mostly positive (Fig. 5d). The vertical profile of the time averaged zonal component of the energy flux shows a minimum near the nodal point of the first baroclinic mode and maxima in the upper and lower layers. The maximum zonal energy flux is ~100 W m^{-2} (Fig. 5f). The depth integrated zonal energy flux also shows a semidiurnal fluctuation, with a mean of ~14 kW m^{-1} averaged over the 28-h period. The depth integrated meridional energy flux is −1 kW m^{-1} (Fig. 5e). In summary, at station I the internal tidal energy flux propagates toward the canyon head following the canyon axis (see white arrow in Fig. 1a). The depth integrated internal tidal energy flux in the canyon mouth of Gaoping Submarine Canyon is more than twice that measured at the mouth of Monterey Canyon, <5 kW m^{-1} (Kunze et al., 2002) and is ten times that found

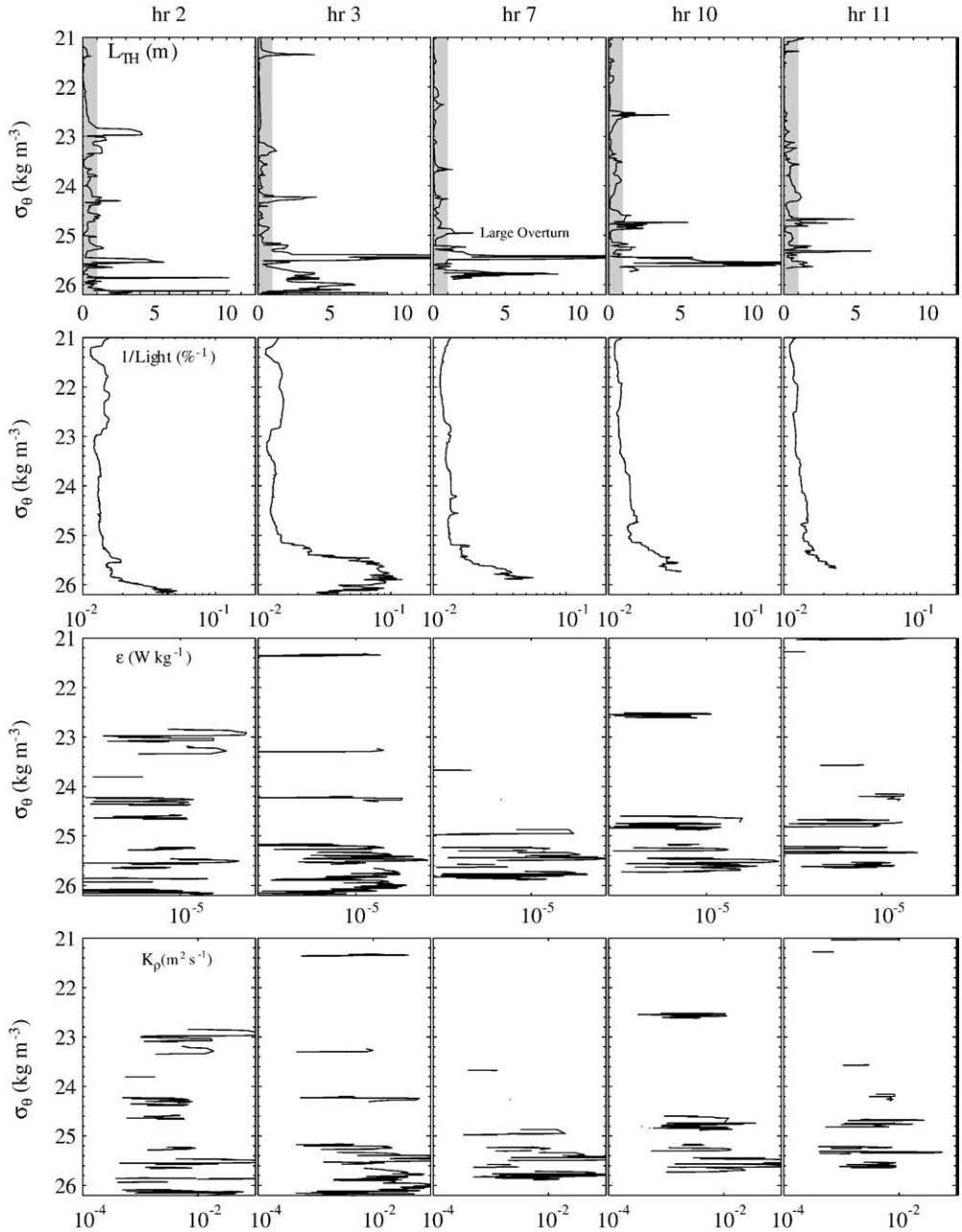

Fig. 8. Profiles of rms Thorpe scales (the top panels), inverse light transmission (the second to the top panels), turbulence kinetic energy dissipation rate (the second from the bottom panels), and the eddy diffusivity (the bottom panels) at five different hours, hours 2, 3, 7, 10, and 11 at isopycnal surfaces. Profiles at hours 3, 7 and 10 correspond to the time of strong turbulence (see Fig. 7).

near the head of Monterey Canyon, 1.5 kW m^{-1} (Carter and Gregg, 2002). The barotropic tidal current in Monterey Canyon is O (0.01 m s^{-1}) (Petruncio et al., 1998). The barotropic tidal current in Monterey Canyon is much weaker than the barotropic tidal current in Gaoping Submarine Canyon, ~0.5 m s^{-1}. Therefore, we expect much stronger internal tidal energy in the canyon than that in Monterey Canyon. The observed internal tidal energy flux is nearly ten times that in the deep basins at western Pacific and near Hawaii, 1–2 kW/m, estimated using historical hydrographic and mooring measurements (Alford, 2003). It is comparable to the observed strong semidiurnal internal tidal energy flux, O (10) kW m^{-1}, radiating from the Hawaiian Ridge (Lee et al., 2006). Note that our results of internal tidal energy and energy flux are estimated from a short 28-h record. They might not be representative as typical characteristics in Gaoping Submarine Canyon. Nonetheless, they represent the possible internal tidal energy and energy flux in the canyon. Further investigations will be needed to quantify the geographical and temporal variation of internal tidal energy and energy flux.

4. Turbulence properties

Turbulent processes are the primary mechanism for resuspension and transport of suspended sediment in the submarine canyon. In Gaoping Submarine Canyon, turbulence could be generated via surface forcing such as typhoons and monsoons, inertial wave breaking in the interior, the barotropic tidal shear near the solid boundary, the breaking of internal tides near the generation sites, and the breaking of internal tides and internal waves near the critical slopes.

We do not have direct turbulence measurements in the canyon. Turbulent overturning Thorpe scales L_T will be estimated based on vertical profiles of CTD. The turbulence kinetic energy dissipation rate ε will be estimated using the relation between Ozmidov scale $L_O=(\varepsilon/N^3)^{1/2}$ (Ozmidov, 1965) and Thorpe scale, $L_O \approx 0.8L_T$ (Dillon, 1982). Accordingly, $\varepsilon \approx 0.64L_T^2N^3$. The turbulence eddy diffusivity is computed using the Osborn method (Osborn, 1980), i.e., $K_\rho=0.2\varepsilon N^{-2}=0.13L_T^2N^{-1}$. Details of turbulence estimates are discussed in the following sections.

4.1. Overturning scales

Thorpe scale L_T is defined as the root-mean-square (rms) of Thorpe displacements of the density profile from its sorted profile (Thorpe, 1977). The vertical resolution of the CTD profile, instrument noise, mismatch response time of temperature and conductivity sensors, and systematic errors could produce spurious estimates of overturning and lead to incorrect estimates of the overturning scale. Galbraith and Kelley (1996) thoroughly discuss the problems of determining overturning scales using vertical profiles of CTD data. They designed a statistical run-length test to exclude possible errors due to the instrument noise and systematic errors. Johnson and Garrett (2004) revisit the run-length test. They conclude that, although the run-length test is a useful diagnostic, comparing the run-length statistics with the uncorrelated random series might not be appropriate for typical oceanic conditions. We will follow Galbraith and Kelley's schemes to determine a threshold for our estimates of Thorpe scales. The run-length statistics will be compared with run-length statistics of the randomly reshuffled density profile, instead of the theoretical value suggested by Galbraith and Kelley (1996).

4.2. Techniques for estimates of Thorpe scales

The vertical resolution of observed CTD profiles δz is 0.2 m. Galbraith and Kelley (1996) suggest that only overturning scales $L>5\delta z=1$ m could be detected. With the strongest stratification $N\sim0.01$ s^{-1}, the lowest bound of estimates of ε is $L^2N^3\sim10^{-6}$ W kg^{-1}. At places of weak stratification $N=0.001$ s^{-1}, we may detect ε as low as 10^{-9} W kg^{-1}. The resolution of density measurements is ~0.001 kg m^{-3}. It sets another limit on the smallest detectable overturning scale, $L_\rho=2g(\delta\rho/\rho_0)/N^2\sim0.02$–2 m for $N=0.01$ and 0.001 s^{-1}, respectively. Combining the constraints of the vertical resolution of CTD profiles and of the density resolution, the smallest detectable overturning scale is ~1 m.

Fig. 6 illustrates the estimate of Thorpe displacement, definition of the overturning patch, the estimate of the rms Thorpe scale, and the run-length test. Each observed vertical profile of potential density is sorted so that the water is stably stratified. The original, unsorted, density profile and the sorted density profile are shown in Fig. 6a. At each depth, the difference between the observed density and the sorted density is called the Thorpe density fluctuation. Thorpe displacement is defined as the vertical distance between the displaced depth and the initial depth. The overturning patch is

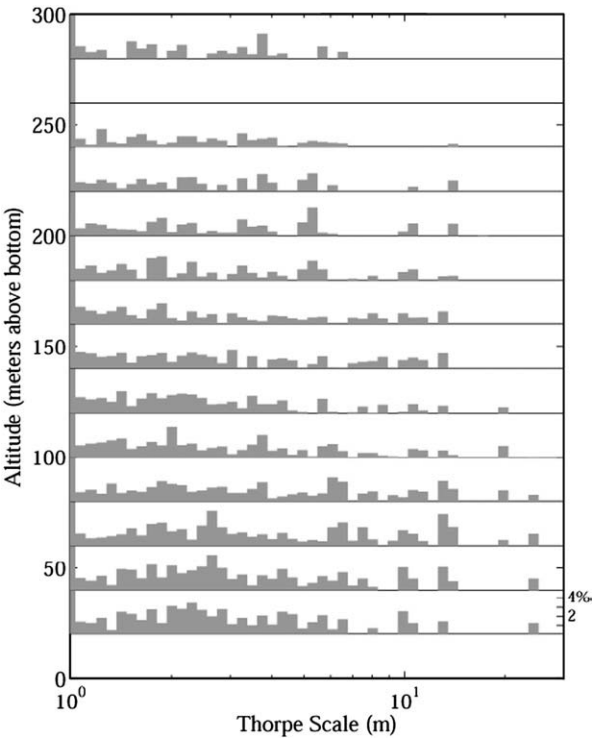

Fig. 9. Histograms of L_T as a function of distance above the bottom. L_T is binned in logarithmic scales in order to see the variation of histograms of small scale L_T. The scale of the histogram is marked on the right axis.

defined such that the accumulated density difference within the patch is smaller than the density resolution $\delta\rho$ (stairs in Fig. 6c). Thorpe scale L_T is defined as the root-mean-square (rms) value of Thorpe displacements within each patch.

Thorpe displacements as large as 30 m are found near the bottom, varying mostly between 1 and 15 m (Fig. 6c). The vertical scale of overturning patches is typically less than 10 m. The largest vertical scale overturning patches is ~35 m found near the bottom.

The run-length test is carried out for all profiles. Detail of the run-length test is discussed in Galbraith and Kelley (1996). The run is defined as a series of adjacent Thorpe displacements of the same sign. The number of points within each run is defined as the run-length.

The probability density function (pdf) of the run-length is computed using the complete vertical profile. For uncorrelated random series, the pdf of a run-length n is 2^{-n} (Larson and Marx, 1986). Johnson and Garrett (2004) suggest that the theoretical pdf, 2^{-n}, may not be appropriate to define the threshold criterion for true density inversion of typical ocean density profiles. We will take an alternative approach. A Monte Carlo simulation is used to compute the pdf of the run-length of randomly reshuffled observed density profiles. The pdf of the run-length of the observed density profile is compared with those computed from randomly reshuffled density profiles. The pdf of the run-length of randomly reshuffled density profiles agrees well with the theoretical prediction for uncorrelated random series. The 95% confidence interval of the pdf of the randomly reshuffled density profiles is adopted as the threshold for the true density overturning. This typical illustration shows that Thorpe scales greater than ~1 m are acceptable as true density overturning. Throughout this analysis, estimates of overturning scales smaller than 1 m will be excluded.

Galbraith and Kelley (1996) use the water-mass test to remove spurious inversions due to intrusions. Within each turbulence patch, a least linear regression is fitted between temperature and density, $\rho_T = a_T + b_T T$, and between salinity and density, $\rho_S = a_S + b_S S$. The sum of rms errors between the observed density ρ and ρ_T, and between ρ and ρ_S are normalized by the rms Thorpe density fluctuations $R = \left[\frac{1}{M}\sum_1^M \rho'^2\right]^{1/2}$, i.e., $R_T = \left[\frac{1}{M}\sum_1^M (\rho-\rho_T)^2\right]^{1/2}/R$ and $R_S = \left[\frac{1}{M}\sum_1^M (\rho-\rho_S)^2\right]^{1/2}/R$, where M is the number of density measurements, and ρ' is Thorpe density fluctuation. We exclude density inversions which have $\mathrm{Max}\{R_T, R_S\} > R_C = 0.5$. The criterion of $R_C = 0.5$ is adopted from Galbraith and Kelley (1996). Each overturning patch is inspected with this test.

4.3. Temporal and vertical distributions of turbulence within Gaoping Submarine Canyon

Thorpe scales are computed using measurements of 12 h of continuous CTD profiles (Fig. 7). Time series of buoyancy frequency, derived turbulence properties and light transmissions are averaged over three density layers, σ_θ=23.2–23.6, σ_θ=25.2–25.6, and σ_θ=26.2–26.6 kg m^{-3}, called the upper,

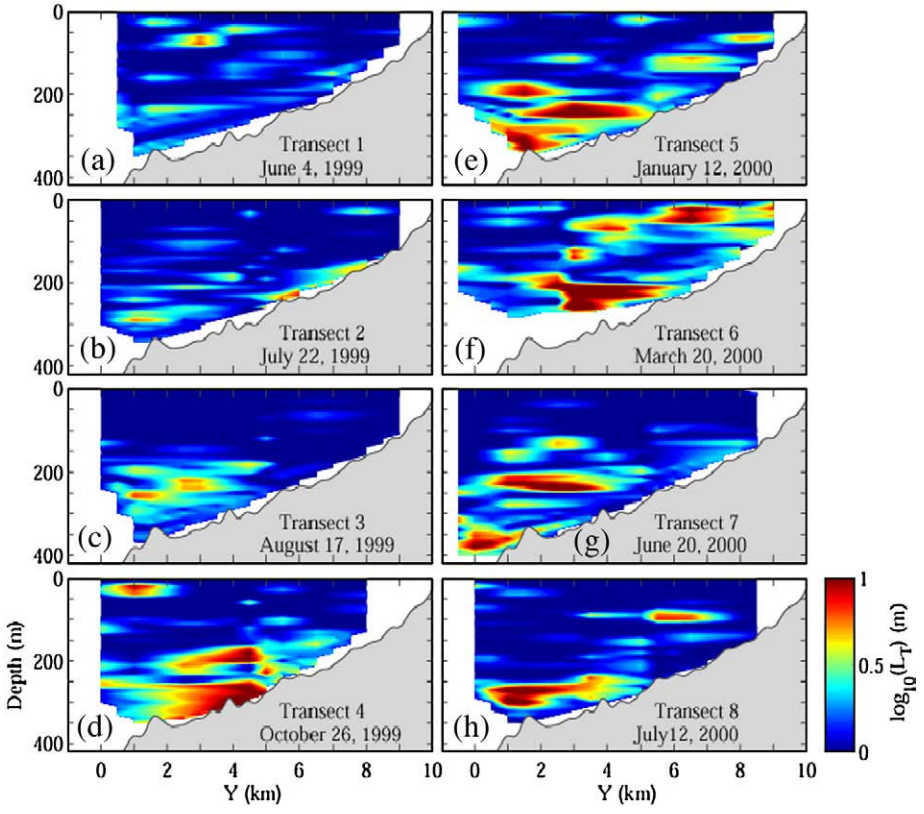

Fig. 10. Estimates of Thorpe Scales during 8 transects along the axis of the Gaoping Submarine Canyon. Estimates of Thorpe scales less than 1 m should be disregarded because they do not pass the run-length-test criterion.

intermediate, and lower layers. The tidal isopycnal displacement during the 12-h period is ~50 m. The buoyancy frequency remains nearly constant in the first 6 h, and varies greatly in the later 6 h. Estimates of $L_T > 5$ m are consistently observed in the intermediate layer with three bursts of 10-, 8-, and 5-m in the 12-h period, and about 2 m in the lower layer. The separation of bursts suggests the turbulence time scale is shorter than 1 h. The associated turbulence kinetic energy dissipation rate, $\varepsilon \approx 0.64 L_T^2 N^3$, exceeds 10^{-4} W kg^{-1} in the intermediate layer during flood tide (rising interface) and $< 10^{-7}$ W kg^{-1} during ebb (descending interface). In the lower layer, it is slightly greater than 10^{-5} W kg^{-1} during flood tide and ~10^{-7} W kg^{-1} during ebb. Two bursts of low light transmission occur in the intermediate and lower layers. The first burst coincides with the burst of strong turbulent overturning, L_T ~ 10 m. The second burst of low light transmission lags the second burst of L_T ~ 8 m by ~2 h. Assuming that particles are stirred up from the bottom by boundary-layer turbulence, light particles could remain floating in the water column even after turbulence decays, whereas heavy particles may settle through the turbulence patches. On the other hand, particles may preferentially settle through quiescent water. Because of the intrinsic differences between the sediment and turbulence dynamics, high concentrations of particles and energetic turbulence do not necessary collocate.

The eddy diffusivity is estimated as $K_\rho = 0.2\varepsilon N^{-2} = 0.13 L_T^2 N^{-1}$. During flood tide, K_ρ exceeds 0.1 m^2 s^{-1} in the intermediate layer. In the lower layer, K_ρ is typically 0.01 m^2 s^{-1}. During ebb, K_ρ decreases to 0.001 m^2 s^{-1}. The 12-h CTD-profile measurements were taken near a week spring tide in June 2000. In Monterey Canyon, Carter and Gregg (2002) find $\varepsilon > 10^{-4}$ W kg^{-1} and K_ρ ~ 0.08 m^2 s^{-1} during the spring tide.

Profiles of L_T, ε, K_ρ, and light transmission along isopycnal surfaces are shown in Fig. 8. Large Thorpe scales, >10 m, clearly exist in the intermediate density layer σ_θ = 25.2–25.6 kg m^{-3}. In hours 2, 3, and 7 (during the flood), large Thorpe scales with low light transmission exist near bottom suggesting resuspension of sediment.

Histograms of L_T as a function of distance above the bottom are shown in Fig. 9. Typical CTD profiles stop 20 m above the bottom. Thorpe scales greater than 10 m are confined to the bottom 2/3 of the water column, suggesting the importance of interior turbulence.

4.4. Spatial and temporal variations of turbulence along and across Gaoping Submarine Canyon

Thorpe scales and turbulence properties are computed using CTD measurements taken in 8 transects along the axis of the canyon (Fig. 10). Thorpe scales greater than 10 m are found near the bends of the canyon axis and near the bottom, especially clear in cruises 5, 6, and 8. Near the mooring station (magenta line), large Thorpe scales are found at mid-depths and near the bottom, most clearly in cruises 1, 5, 6, 7, and 8. This is consistent with results found in the previous section.

The estimate of eddy diffusivity along the canyon axis during 8 transects is shown in Fig. 11. Large eddy diffusivity occurs near the bends of the canyon axis, as large as 0.1 m^2 s^{-1},

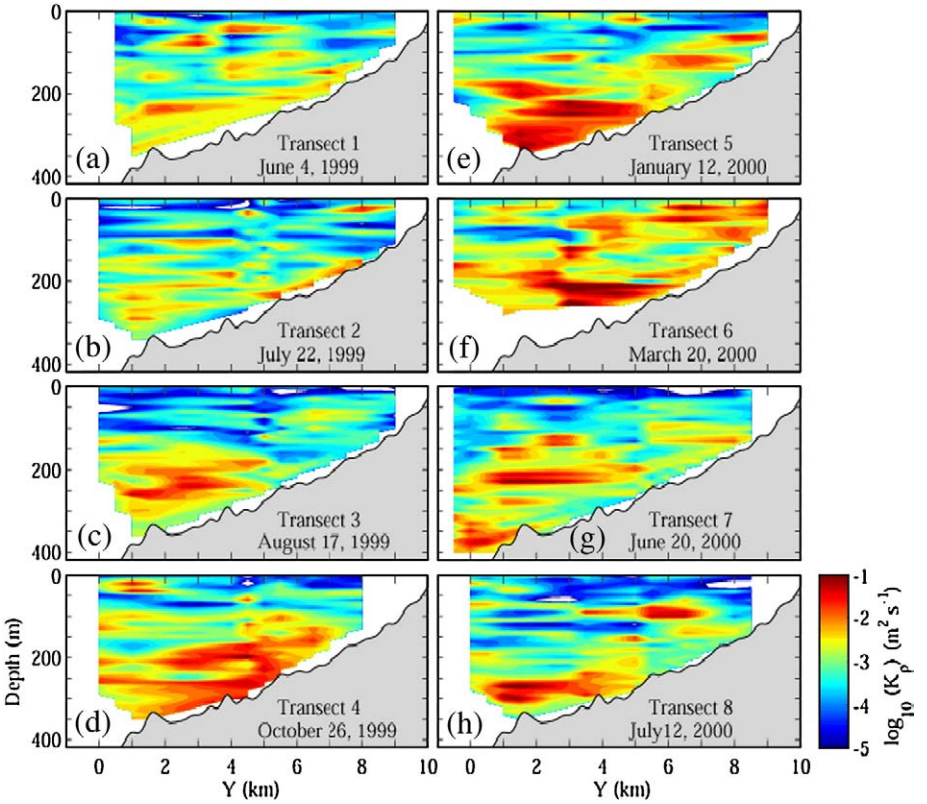

Fig. 11. Estimates of eddy diffusivity during 8 transects along the axis of the Gaoping Submarine Canyon.

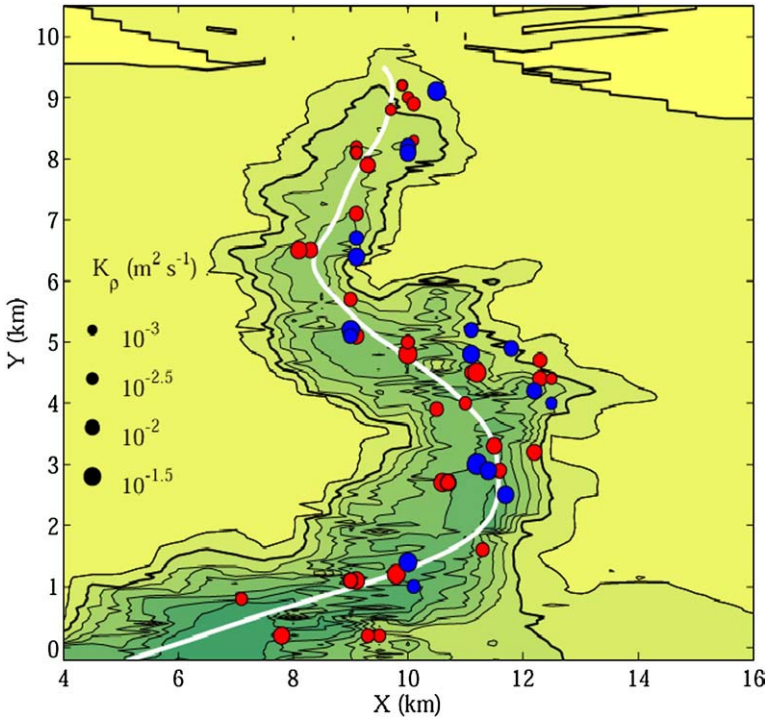

Fig. 12. Geographical distribution of the vertically averaged eddy diffusivity $\bar{K}_\rho$ (dots) in two winter cruises (blue) and in six summer and fall cruises (red). The size of dots represents the magnitude of $\bar{K}_\rho$. The scale reference is represented as sizes of black dots on the left of the plot. Black curves represent isobath of 50 m interval. The white curve marks the center axis of the Gaoping Submarine Canyon estimated as the low-pass filter of positions where the water is the deepest.

and near the bottom, mostly 0.01 m^2 s^{-1}. In cruise 7, the eddy diffusivity near the mooring station (magenta line) has a maximum of ~0.05 m^2 s^{-1} at 150–200 m depth, a similar magnitude found in the previous section (Figs. 7 and 8).

The spatial distribution of the depth averaged eddy diffusivity is shown in Fig. 12. In summer and fall, the eddy diffusivity varies between 0.001 and 0.034 m^2 s^{-1}, with a mean of 0.008 m^2 s^{-1}. In winter, the eddy diffusivity varies between 0.003 and 0.061 m^2 s^{-1}, with a mean 0.019 m^2 s^{-1}. The eddy diffusivity in winter is twice that of summer and fall.

In winter, the depth averaged eddy diffusivity along the canyon axis varies in 0.01–0.04 m^2 s^{-1} within 9 km from the

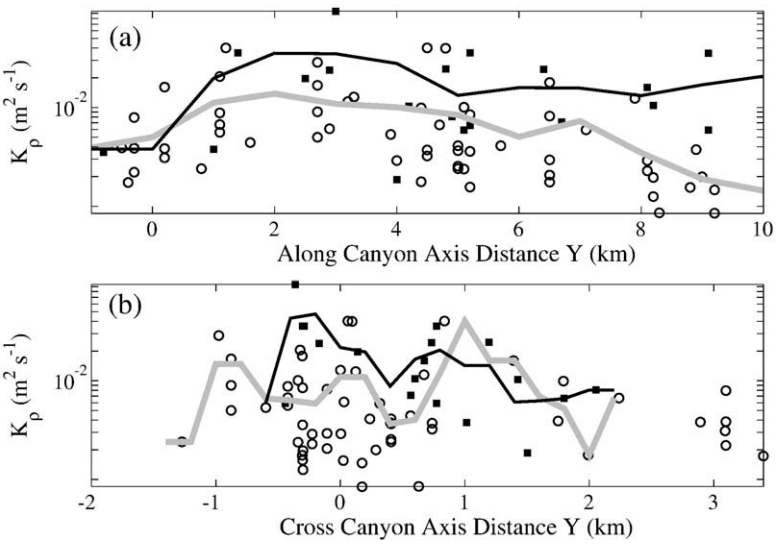

Fig. 13. Summary of estimates of eddy diffusivity along the canyon axis (a), and cross canyon axis (b). Filled squares are estimates taken in two winter cruises, and circles are estimates taken in six summer and fall cruises. The black curve is the mean for winter cruises, and the gray curve is the mean for summer and fall cruises. Note that the mouth of the canyon is at Y=0 km and the head is at Y=10 km.

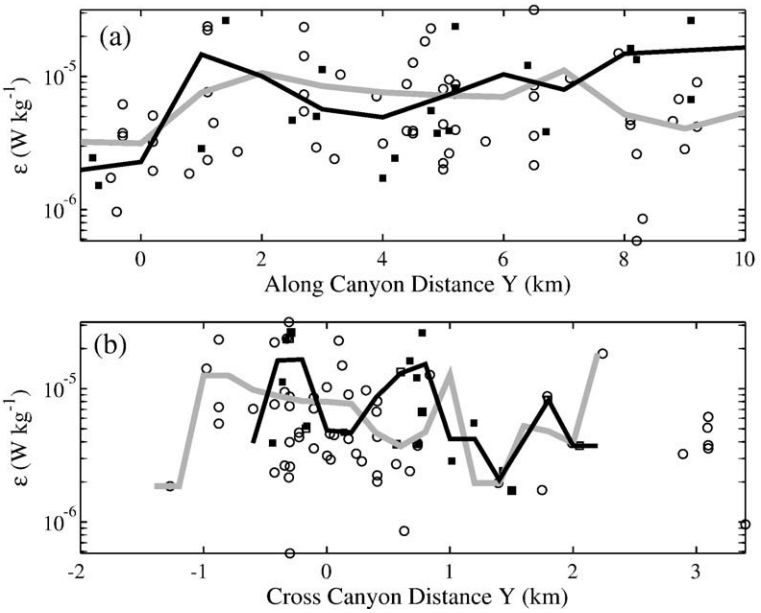

Fig. 14. Summary of estimates of turbulence kinetic energy dissipation rate ε along the canyon axis (a), and cross canyon axis (b). Filled squares are estimates taken in two winter cruises, and circles are estimates taken in six summer and fall cruises. The black curve is the mean for winter cruises, and the gray curve is the mean for summer and fall cruises. Note that the mouth of the canyon is at Y=0 km and the head is at Y=10 km.

canyon head, i.e., Y>1 km, and drops by a factor of ~10 in 1 km to 0.004 $m^2\ s^{-1}$ near the canyon mouth (Fig. 13). In summer and fall, the depth averaged eddy diffusivity increases from 0.0015 $m^2\ s^{-1}$ at the canyon head to 0.01 $m^2\ s^{-1}$ at 1 km from the canyon mouth, and drops by a factor of 3 in 1 km to 0.004 $m^2\ s^{-1}$ near the canyon mouth, similar to the winter condition. The largest eddy diffusivity exists in 1–4 km from the canyon mouth. There is no clear cross-canyon structure of eddy diffusivity (Fig. 13b). In all seasons, the eddy diffusivity seems to decrease slightly beyond ~1 km off the canyon axis.

There is no significant seasonal variation of the depth averaged ε (Fig. 14). The two times larger eddy diffusivity in winter than in summer and fall is due to the weaker stratification in winter. The depth averaged ε varies in 4–10×10^{-6} W kg^{-1} within 9 km from the canyon head, Y>1 km, and drops by about a factor of 5 in 1 km at the canyon head. There is a slight decrease of ε beyond 1 km off the canyon axis. The bulk estimate of the depth integrated turbulence kinetic energy dissipation rate in Gaoping Submarine Canyon is O (1) W m^{-2}, which is 1000 times of that estimated in the global abyssal ocean, 1 m W m^{-2}, and that expected for the GM internal wave model, 0.8 mW m^{-2} (Kunze et al., 2006).

5. Discussions

It is worthwhile to compare our estimates of turbulence intensity in KPSC with those directly measured in Monterey Canyon (Carter and Gregg, 2002; Gregg et al., 2005). Averaged within 10 km of the head of Monterey Canyon, the kinetic energy dissipation rate ε is 1.9×10^{-7} W kg^{-1}, and the eddy diffusivity is 0.0025 $m^2\ s^{-1}$. The measured ε in Monterey Canyon is 1 decade smaller than that in Gaoping Submarine Canyon. The eddy diffusivity near the head of the Monterey Canyon is a factor of 4–16 of that estimated within 9 km of the head of Gaoping Submarine Canyon. In both Gaoping Submarine Canyon and Monterey Canyon, turbulence is stronger on the canyon axis, and weaker off the axis. Within a ~50-m thick layer of an internal tidal beam over a sea fan in Monterey Bay, off the canyon, ε exceeds 10^{-6} W kg^{-1}, and K_ρ exceeds 0.01 $m^2\ s^{-1}$ (Lien and Gregg, 2001).

Our estimate of internal tidal energy near the mouth of Gaoping Submarine Canyon is 0.17 $m^2\ s^{-2}$, likely overestimated as explained in 3.2. Assuming that the internal tidal energy is dissipated in one semidiurnal period, the kinetic energy dissipation rate is 4×10^{-6} W kg^{-1}. The estimate of depth integrated internal tidal energy flux near the mouth of the canyon is 14 kW m^{-1}, propagating into the canyon head (Fig. 1a). A bulk estimate of turbulence kinetic energy dissipation rate is $\sim7\times10^{-6}$ W kg^{-1}, assuming a balance between the energy flux divergence and the turbulence kinetic energy dissipation rate, i.e., $\varepsilon\approx\tilde{F}W_k/(L_kH_kW_k\rho_0)\equiv\tilde{F}/(L_kH_k\rho_0)$, where W_k is the average width, H_k the average depth, and L_k the distance from the station of the internal tidal energy estimate to where the internal tidal energy flux diminishes. $\tilde{F}$ is the depth integrated internal tidal energy flux. We assume that internal tidal energy flux diminishes at the canyon head, i.e., L_k=10 km, and the average depth within 10 km of the canyon head is H_k=200 m. These two bulk estimates, 4×10^{-6} W kg^{-1} and 7×10^{-6} W kg^{-1}, suggest that internal tides in Gaoping Submarine Canyon alone may provide energy sufficient to explain the observed turbulence intensity in the canyon, 4–10×10^{-6} W kg^{-1}.

6. Summary

Our analysis provides first estimates of internal tidal energy, internal tidal energy flux, turbulence kinetic energy

dissipation rate, and eddy diffusivity in one of the major canyons in Taiwan, Gaoping Submarine Canyon. Both barotropic and baroclinic tides are strong and have nearly equal speed of ~0.5 m s^{-1}. The baroclinic tide shows a clear first mode structure. The depth integrated baroclinic tidal energy flux is 14 kW m^{-1} at the canyon mouth, and is 3–7 times of that measured in Monterey Canyon (Kunze et al., 2002; Carter and Gregg, 2002). The depth averaged baroclinic tidal energy is 0.17 m^2 s^{-2}. Simple energy budget calculations conclude that internal tides alone could provide energy sufficient to explain the turbulent mixing observed in Gaoping Submarine Canyon.

Thorpe scales are computed using CTD vertical profiles with a minimum threshold of 1 m determined by the modified run-length test. Thorpe scales greater than 10 m exist in the bottom 2/3 of the water column. Bursts of strong turbulence and low light transmission are found in a mid-depth density layer, with $\varepsilon > 10^{-4}$ W kg^{-1} and $K_\rho > 0.1$ m^2 s^{-1}, suggesting the low light transmission resulted from the sediment resuspension by turbulence entrainment.

Within the canyon, the depth averaged ε is ~7×10^{-6} W kg^{-1} and K_ρ is ~0.01 m^2 s^{-1}. The turbulence drops by about five times near the canyon mouth. There appears to be no significant seasonal variation of ε.

Further investigations of internal tides and sediment transport are necessary. We expect a significant seasonal variation of internal tidal energy and energy flux in the canyon because a strong seasonal variation of stratification in the canyon has been reported (Liu et al., 2002). To understand the effects of internal tides on the sediment transport, we need detailed measurements of internal tides along and across canyon axis.

Acknowledgements

The funding for this study was provided by the R.O.C. National Science Council (NSC) under grant numbers: NSC87-2611-M-110-002, NSC88-2611-M-110-001, NSC89-2611-M-110-015, NSC90-2611-M-110-007, and NSC 92-2611-M-110-012. NSC also provided additional funding for J.T. Liu to visit the Applied Physics Laboratory of University of Washington to initiate this collaboration and the follow-up visit by I.-H. Lee for extended work. We would like to give our special thanks to crews of *R/V* Ocean Researcher III. Without their skillful help, these precious measurements could not have been taken. We greatly appreciate Dr. Eric Kunze for his critical comments, constructive suggestions, and careful reviews. His help has improved the presentation of this work. We also want to thank the other anonymous reviewer for his helpful comments and suggestions to improve the manuscript.

References

Alford, M.H., 2003. Redistribution of energy available for ocean mixing by long-range propagation of internal waves. Nature 423, 159–163.
Carter, G.S., Gregg, M.C., 2002. Intense, variable mixing near the head of Monterey submarine canyon. Journal of Physical Oceanography 32, 3145–3165.
Cresswell, G.R., 2000. Coastal currents of northern Papua New Guinea, and the Sepik River outflow. Marine and Freshwater Research 51, 553–564.
Dillon, T.M., 1982. Vertical overturns: a comparison of Thorpe and Ozmidov length scales. Journal of Geophysical Research 87, 9601–9613.
Friedrichs, C.T., Wright, L.D., 1995. Resonant internal waves and their role in transport and accumulation of fine sediment in Echernforde Bay, Baltic Sea. Continental Shelf Research 15, 1697–1721.
Galbraith, P.S., Kelley, E., 1996. Identifying overturns in CTD profiles. Journal of Atmospheric and Oceanic Technology 13, 688–702.
García Lafuente, J., Sarhan, T., Vargas, M., Vargas, J.M., Plaza, F., 1999. Tidal motions and tidally induced fluxes through La Linea submarine canyon, western Alboran Sea. Journal of Geophysical Research 104 (c2), 3109–3119.
Garrett, C.J.R., Munk, W.H., 1972. Space-time scales of internal waves. Geophysical Fluid Dynamics 3, 225–264.
Garrett, C.J.R., Munk, W.H., 1975. Space-time scales of internal waves: a progress report. Journal of Geophysical Research 80, 291–297.
Gregg, M.C., Carter, G.S., Kunze, E., 2005. Corrigendum. Journal of Physical Oceanography 35, 1712–1715.
Henyey, F.S., 1983. Hamiltonian description of stratified fluid dynamics. Physics of Fluids 26, 40–47.
Hotchkiss, F.S., Wunsch, C., 1982. Internal waves in Hudson Canyon with possible geological implications. Deep-Sea Research 29, 415–442.
Jachec, S.M., Fringer, O.B., Gerritsen, M.G., Street, R.L., 2006. Numerical simulation of internal tides and the resulting energetics within Monterey Bay and the surrounding area. Geophysical Research Letters 33, L12605. doi:10.1029/2006GL026314.
Johnson, H.L., Garrett, C., 2004. Effects of noise on Thorpe scales and run-length. Journal of Physical Oceanography 34, 2359–2372.
Kunze, E., Rosenfeld, L.K., Carter, G.S., Gregg, M.C., 2002. Internal waves in Monterey submarine canyon. Journal of Physical Oceanography 32, 1890–1913.
Kunze, E., Firing, Hummon, J.M., Chereskin, T.K., Thurnherr, A.M., 2006. Global abyssal mixing inferred from lowered ADCP shear and CTD strain profiles. Journal of Physical Oceanography 36, 1553–1576.
Larson, R.J., Marx, M.L., 1986. An Introduction to Mathematical Statistics and its Application, 2nd ed. Prentice-Hall Inc., Upper Saddle River, NJ.
Lee, C.M., Kunze, E., Sanford, T.B., Nash, J.D., Merrifield, M.A., Holloway, P.E., 2006. Internal tides and turbulence along the 3000-m isobath of the Hawaiian Ridge. Journal of Physical Oceanography 36, 1165–1183.
Lien, R.C., Gregg, M.C., 2001. Observations of turbulence in a tidal beam and across a coastal ridge. Journal of Geophysical Research 106, 4575–4591.
Lien, R.C., Tang, T.Y., Chang, M.H., D'Asaro, E.A., 2005. Energy of nonlinear internal waves in the South China Sea. Geophysical Research Letters 32, L05615. doi:10.1029/2004GL022012.
Liu, J.T., Liu, K.-J., Huang, J.C., 2002. The influence of a submarine canyon on river sediment dispersal and inner shelf sediment movements: a perspective from grain-size distributions. Marine Geology 181 (4), 357–386.
McPhee-Shaw, E.E., Kunze, E., 2002. Boundary layer intrusion from a sloping bottom: a mechanism for generating intermediate nepheloid layers. Journal of Geophysical Research 107 (C6), 3050. doi:10.1029/2001JC000801.
Monaco, A., Biscaye, P., Soyer, J., Pocklington, R., Heussner, S., 1990. Particulate fluxes and ecosystem response on a continental margin: the 1985–1988 Mediterranean ECOMARGE experiment. Continental Shelf Research 10 (9–11), 809–839.
Osborn, T.R., 1980. Estimates of the local rate of vertical diffusion from dissipation measurements. Journal of Physical Oceanography 10, 83–89.
Ozmidov, R.V., 1965. On the turbulent exchange in a stably stratified ocean. Izvestiya Academy of Sciences, USSR. Atmospheric and Oceanic Physics I, 861–871.
Petruncio, E.T., Rosenfeld, L.K., Paduan, J.D., 1998. Observations of the internal tide in Monterey Canyon. Journal of Physical Oceanography 28, 1873–1903.
Ribbe, J., Holloway, P.E., 2001. A model of suspended sediment transport by internal tides. Continental Shelf Research 21, 395–422.
Shepard, F.P., Marshall, N.F., McLoughlin, P.A., 1974. "Internal waves" advancing along submarine canyons. Science 183 (4121), 195–198. doi:10.1126/science.183.4121.195.
Shepard, F.P., Marshall, N.F., McLoughlin, P.A., Sullivan, G.G., 1979. Currents in submarine canyons and other sea valleys. AAPG Studies in Geology. American Assoc. of Petroleum Geologists, vol. 8. 173 pp.
Thorpe, S.A., 1977. Turbulence and mixing in a Scottish Loch. Philosophical Transactions of the Royal Society of London, Series A 286, 125–181.
Wunsch, C., 1976. Geographical variability of the internal wave field: a search for sources and sinks. Journal of Physical Oceanography 6 (4), 471–485.
Wunsch, C., Webb, S., 1979. The climatology of deep ocean internal waves. Journal of Physical Oceanography 9, 235–243.
Xu, J.P., Noble, M., Eittreim, S.L., Rosenfeld, L.K., Schwing, F.B., Pilskaln, C.H., 2002. Distribution and transport of suspended particulate matter in Monterey Canyon, California. Marine Geology 181, 215–234.